

FINITE ELEMENT ANALYSIS ON THE FATIGUE DAMAGE UNDER COMPRESSION OF A CONCRETE SLAB TRACK

ELISA POVEDA*, RENA C. YU, JUAN C. LANCHI, AND GONZALO RUIZ

*E.T.S. de Ingenieros de Caminos, C. y P., Universidad de Castilla-La Mancha (UCLM)
Avda. Camilo José Cela s/n, 13071 Ciudad Real, Spain
e-mail: elisa.poveda@uclm.es, www.uclm.es

Key words: Fatigue under compression, concrete slab track, high-speed train

Abstract. With the growing use of high speed trains, non-ballasted track has become more popular, in spite of its higher construction cost compared to ballasted track. This work studies the fatigue behavior of a slab track using the finite element method. According to Tayabji and Bilow, our slab track system can be classified as a two-slab layer system: a precast reinforced concrete plate and a concrete base, separated by a cement-asphalt-mortar sandwich layer. The entire slab track structure and the soil sub-base are modeled as 3D solid elements, the UIC60 rail represented as truss elements is attached to the surface slab through the fastening devices. A three-slab track system is modeled to reduce the boundary effects, though we only focus on the response of the central slab. Modal analysis is performed to determine the natural frequencies and mode shapes of the system. Real high-speed train pulses are applied to the rail to carry out the transient analysis. Most unfavorable nodes or regions are identified for cycle counting, meanwhile the number of cycles causing fatigue failure at each stress level is estimated according to the new FIB Model Code. Parametric analyses are carried out to evaluate the influence of different geometrical and mechanical factors on accumulated damage. Minimum requirement for material strength and slab thickness is proposed according to the current study.

1 INTRODUCTION

Slab track, also called ballastless track, is a modern form of track construction which has been used successfully throughout the world for high speed lines, heavy rail, light rail and tram systems, for an incomplete list see [1–12] and the references within. Compared to ballasted track, concrete slab track offers a greater degree of trackbed stability, therefore higher running speeds are achievable. Depending on the spectrum of the train loading, the dynamic response of a railway slab track can be significantly larger than its static counterpart. Under such circumstances, a complete dynamic analysis of the slab structure is necessary in order to predict the service life of the constructed track. Pre-

vious dynamic studies have been concentrated on the vehicle-track coupled system [7, 13]. In this current work, we model a three-slab track system, together with its cement-asphalt mortar base, the concrete roadbed and supporting soil. Then we proceed to extract its modal response and carry out the transient analysis applying a real time train load. Fatigue analysis is performed as the post-processing of the transient response. Since the concrete slab is heavily reinforced, we consider fatigue damage at compressive range is more relevant. Cycle counting is based on the rainflow algorithm [14]. Damage map is drawn for one passage of the train, slab life is calculated according to the most unfavorable region.

The rest of the paper is structured as follows: the finite element method is described in Section 2, dynamic analysis including modal analysis, transient calculations and fatigue analysis are all carried out in Section 3, results for real high-speed trains in Section 4 and parametric analysis in Section 5. Finally, relevant conclusions are drawn in Section 6.

2 FINITE ELEMENT METHOD

In this section, we set out to model the slab track superstructure using the ANSYS Parametric Design Language (APDL), a script language to automate common tasks and build complicated finite element models in terms of variables [15].

2.1 Geometry and boundary conditions

Taking advantage of the track line symmetry (x-axis), half of the track geometry is represented. In order to reduce the boundary effects, three slabs were modeled, but only data from the central slab were extracted for the fatigue analysis in Section 3. The slab in-plane dimension is shown in Fig.1(down). Neighboring slabs are separated by a cylindrical bollard to prevent lateral and longitudinal movements. The slab, the cement asphalt mortar (CAM) layer, the concrete roadbed and the soil sub-base are all discretized as 8-node volumetric elements (SOLID45), see Fig. 1(up). The vertical and transversal dimensions for each constituent layer are given in Tab. 1.

It needs to be pointed out that the Vossloh rail-fastening device [16] has been simplified in the following way. The fastening cushion, which is a rubber square pad with an edge length of 0.35 m, is represented as deformable solids, while the fastening mechanism is modeled through connecting the rail inferior nodes to the slab surface below the rubber pad. Meanwhile, no-sliding constraint is imposed between the rubber pad and the slab surface.

The UIC 60 rail cross-section profile, see Fig. 2, is modeled as beam elements (BEAM188) with its proper section. Its dimension and section properties are the known

properties for this kind of profile [2]. The cited beam element in ANSYS is well-suited for linear, large rotation, it includes shear-deformation effects and provides options for unrestrained warping and restrained warping of cross-sections. Above all, it allows us to input the exact cross-section profile for UIC 60. A rail length of 15.53 m which covers the three-slab track system is modeled and symmetry boundary conditions are imposed on both ends.

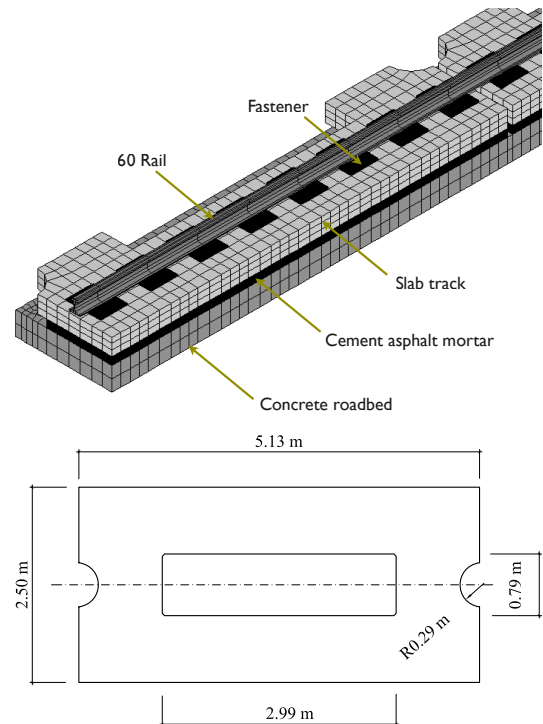


Figure 1: Components of the slab track structure (up) and in-plane dimension in meters of an individual slab (down).

Table 1: Vertical and transversal dimension of the FEM model for each component layer

Layer	Vertical dim. (z-axis) (m)	Transversal dim. (y-axis) (m)
Slab track	0.22	1.25
CA mortar	0.10	0.85
Concrete roadbed	0.30	1.25
Soil subgrade	6.30	7.55
Fastening Cushion	0.02	0.45



Figure 2: The cross-section profile of the UIC60 rail-fastening device seen within the experimental setup to measure its stiffness.

An example of the complete finite element model is given in Fig. 3. Note that the mesh size has been carefully designed to reduce the computational cost.

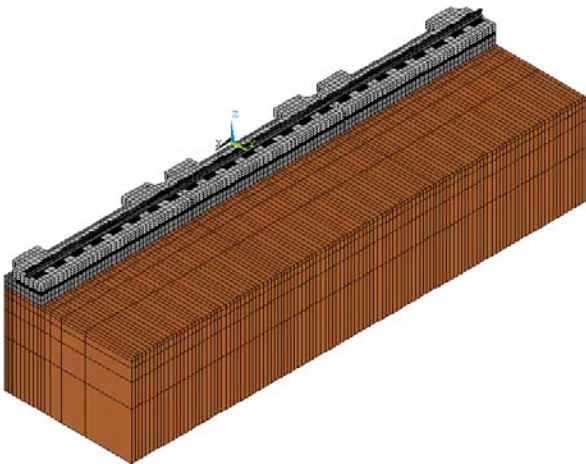


Figure 3: The three-dimensional finite element model for the 3-slab track structure.

2.2 Material characterization

All the solid elements are modeled as linear elastic material with a stiffness-proportional Rayleigh damping coefficient β . The damping factor ζ is fed as the percentage of the material's critical damping ζ_c . For instance, consider an ideal mass-spring-damper system with mass m , spring constant k and viscous damper of damping coefficient c subjected to an oscillatory force, the differential equation for the corresponding homogeneous system is

$$\ddot{x} + 2\zeta\omega_0\dot{x} + \omega_0^2 x = 0 \quad (1)$$

where

$$\omega_0 = \sqrt{\frac{k}{m}} \quad \text{and} \quad \zeta = \frac{c}{2\sqrt{km}} \quad (2)$$

are the undamped natural angular frequency and the damping coefficient respectively. In the case of stiffness-proportional damping ζ can be written as

$$\zeta = \frac{c}{2\sqrt{km}} = \frac{\beta k}{2\sqrt{km}} = \frac{1}{2}\beta\omega_0 \quad (3)$$

The input parameter β is inputted as $2\zeta/\omega_0$. When $\zeta = 1$, the system is critically damped. However for a complex system which has many degrees of freedom thus many modes of vibration, we can only select certain vibration modes to be more damped than others. Therefore, knowing ζ is a percentage to the material's critical damping coefficient, whose estimated value is listed in Tab. 2 for each component material, ω_0 is set to be the frequency that has the maximum amplitude in the train load. For the pulse shown in Fig. 5, the corresponding frequency is of 3.3 Hz.

When the concrete slab was casted, cylinder specimens were also made for standard characterization tests to measure the elastic modulus, tensile strength and compressive strength, all are listed in Tab. 2.

Table 2: Material properties for each constituent element

	f_c (MPa)	f_t (MPa)	E (GPa)	ν	ρ (kg/m ³)	ζ (%)
Concrete slab	35	4	35	0.2	2500	1
CA mortar	-	-	0.1	0.3	1700	10
Concrete roadbed	-	-	35	0.2	2500	1
Soil subgrade	-	-	10-57	0.3	1800	5
UIC 60 Rail	-	-	200	0.3	7850	0.1
Fastening cushion	-	-	0.006	0.3	800	10

The soil sub-grade is also modeled as a linear elastic material but with its stiffness increases with the depth as follows

$$E = E_0 + E_h \times z \quad (4)$$

where z is the average layer depth in meters, E_0 and E_h are of 10 MPa and 10 MPa/m respectively. Fixed boundary conditions are set for both transversal and longitudinal directions. A parametric study was carried out to determine a reasonable soil depth of 6.3 m to be included in the slab track structure. As we have mentioned before, the rail-fastening device has been simplified, only the fastening cushion is modeled as solid elements. Since the stiffness of the fastening device, measured through the experimental setup as shown in Fig. 2, is around 70 kN/mm, an equivalent elastic modulus of 6 MPa (listed in Tab. 2) is assigned to the fastening cushion to achieve a comparable stiffness.

The rest of the material properties in Tab. 2, are all estimated values.

3 DYNAMIC ANALYSIS

In this section, we carry out the dynamic analysis in three steps. First the modal analysis is performed to get the important natural modes and corresponding shapes, above all those with a lower frequency. Second, a real high-speed train load history is applied to the rail to obtain the transient response. Third, fatigue damage is evaluated as the accumulative value according to Miner's summation rule.

3.1 Modal Analysis

Modal analysis is the study of the dynamic properties of structures under vibrational excitation, it uses a structure's overall mass and stiffness to find the various periods that it will naturally resonate at. Detailed modal analysis determines the fundamental vibration mode shapes and corresponding frequencies. For res-

onance to occur, both the mode shape and frequency of the external excitation have to coincide with that of the structure. In Fig. 4, we give the first four modes of vibration of the slab track superstructure and the soil sub-grade. Except the third mode, which represents the settlement of the track structure, the other three modes describe the bending load at different wave length. Special care has to be taken if the external train load has similar shape and spectrum.

3.2 Transient Analysis

Transient dynamic analysis is a technique used to determine the dynamic response of a structure under a time-varying load. In this type of analysis the inertia or damping effects of the structure are considered to be important. In this section, we apply a real high-speed train pulse to the rail to carry out the transient analysis. Figure 5(a) shows the load pulse of a high-speed train (type ETR-Y, see [17]), which is composed of two locomotives and ten coaches and has a total length of 295.4 m. The train runs with a speed of 300 km/h. By means of a Fourier transform, this load pulse is decomposed into its constituent frequencies, see Fig. 5(b). Figure 6 shows the evolution of maximum equivalent stress and deflection in the central slab, note that these maximum values may correspond to different nodes in the slab. The global maximum of the stress and the deflection occurs at 0.224 s and 3.732 s respectively. The maximum equivalent stress of 0.64 MPa is achieved at 0.224 s around the interior corner. The stress and deflection distribution of the central slab at this instant is shown in Fig. 7.

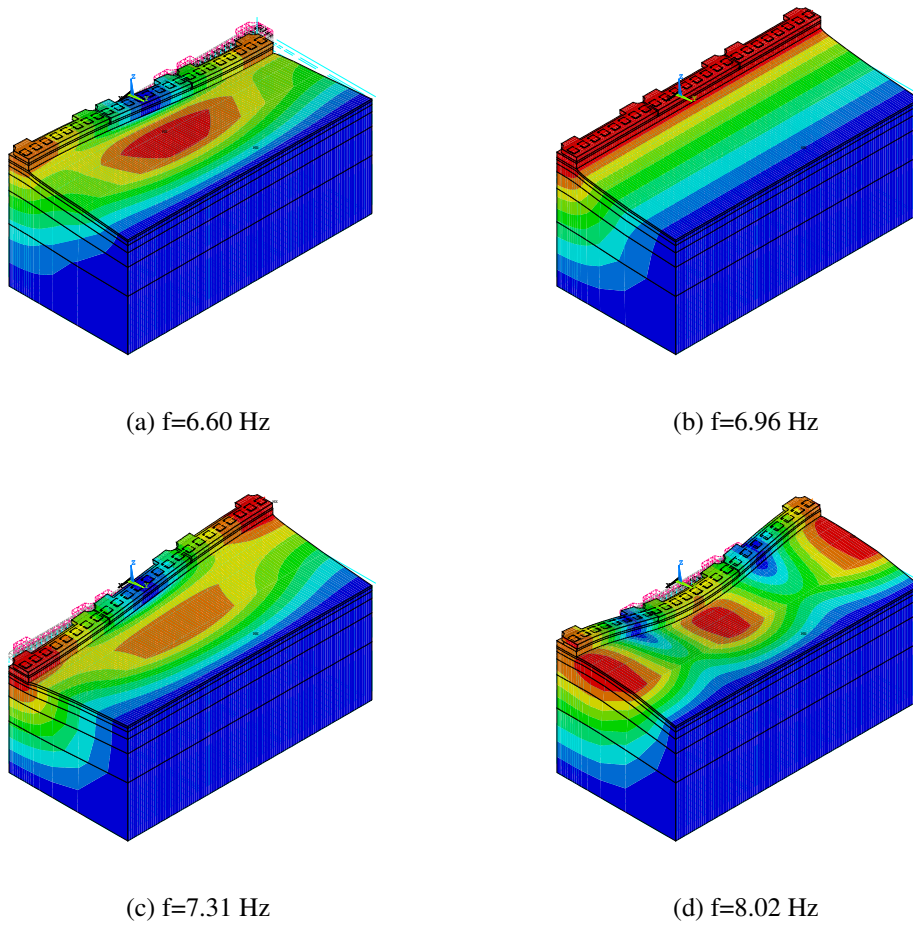


Figure 4: The first four modes of free vibration.

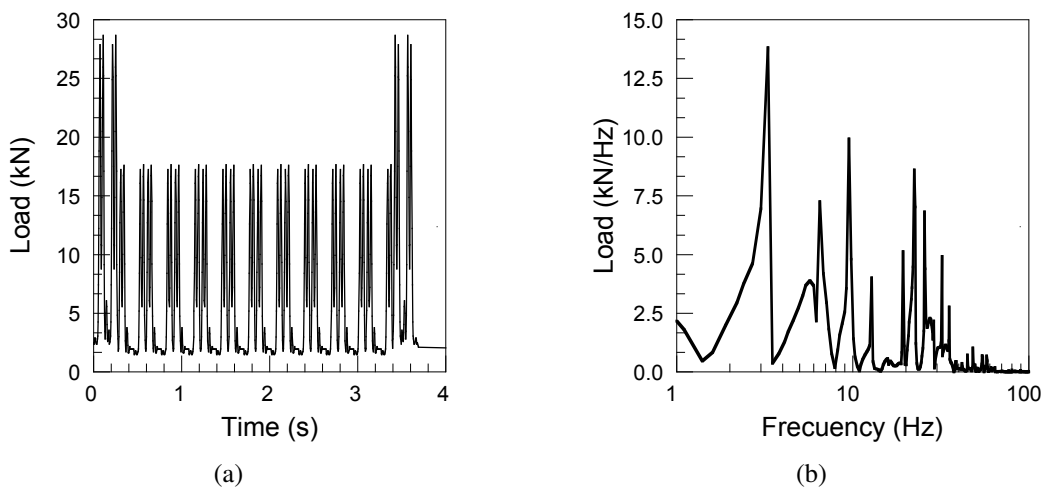


Figure 5: (a) A high-speed train (ETR-Y) load pulse measured at a rail fastening device and (b) its frequency spectrum.

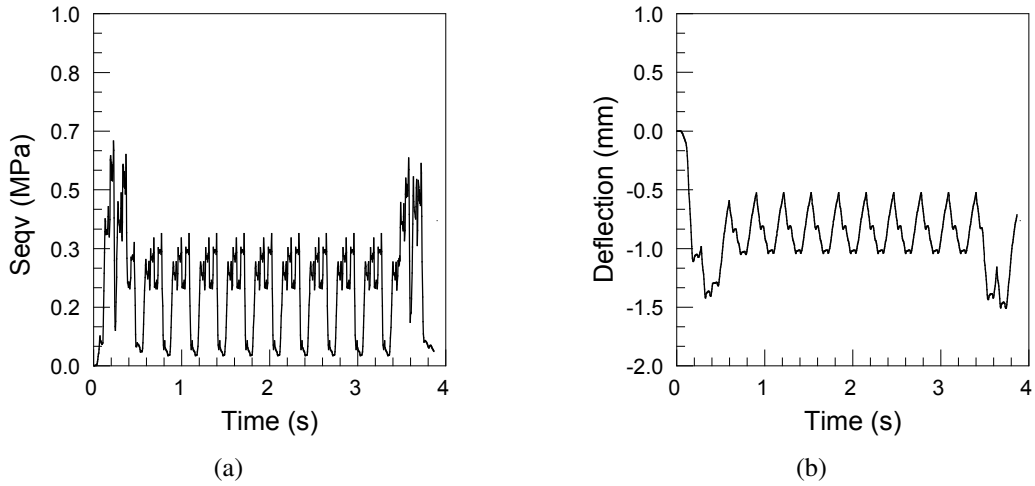


Figure 6: Evolution of the maximum equivalent stress and deflection versus time in the central slab (loaded with the train pulse ETR-Y).

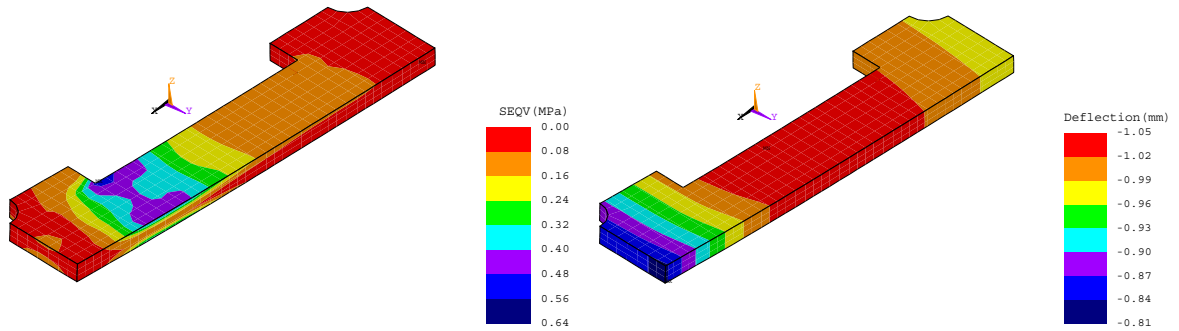


Figure 7: Distribution of the equivalent stress and deflection at loading time 0.224 s (loaded with the train pulse ETR-Y).

3.3 Fatigue damage evaluation

We concentrate on evaluating the damage in the central slab due to compressive stresses. First we extract the third principal stress (and its principal direction) to determine the most unfavorable node or region, the one that suffers the maximum compressive stress during the entire loading duration. Next, taking this principal direction as a reference, the corresponding stress at this direction σ_c and its time history is obtained and plotted in Fig. 8(a). Additionally shown in Fig. 8(a) are the three principal stresses, the equivalent stress and the three normal stresses. It needs to be pointed out that, in order to achieve certain level of damage, the load-pulse in Fig. 5 has been amplified by a fac-

tor 5 to get the results in Fig. 8.

Cycle counting is carried out for the compressive stress σ_c by means of the rain-flow algorithm developed by Downing and Socie [14]. A subroutine is developed to perform this task and to represent the counted cycles as the matrix shown in Fig. 8(b) for each stress range and mean. Taking the characteristic compressive strength f_{ck} as a reference, the design fatigue strength $f_{cd,fat}$ for compression is estimated according to the new Model Code [18] as follows,

$$f_{cd,fat} = 0.85\beta_{cc}(t) \left[f_{ck} \left(1 - \frac{f_{ck}}{25f_{ck0}} \right) \right] / \gamma_c \quad (5)$$

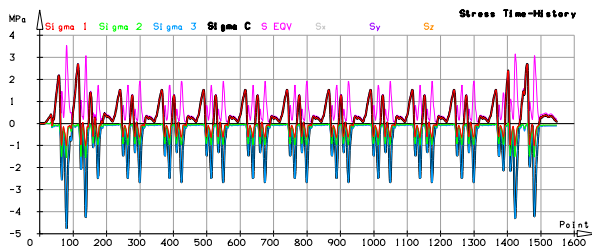
where f_{ck0} is the reference characteristic

strength of 10 MPa, γ_c is a partial security coefficient equals to 1.5, $\beta_{cc}(t)$ is a factor depending on the age of concrete at the beginning of fatigue loading and can be calculated as

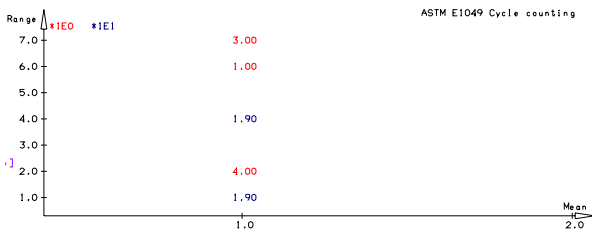
$$\beta_{cc}(t) = \exp \left[s f_{ck} \left(1 - \frac{28}{t} \right)^{1/2} \right] \quad (6)$$

where t is the concrete age in days and s is the coefficient which depends on the strength class of cement concrete [18].

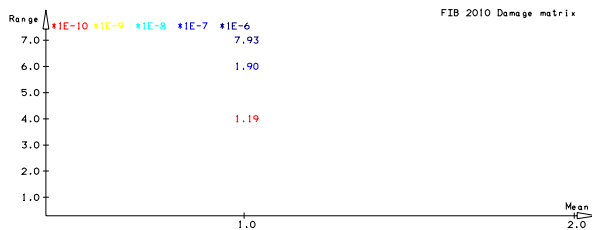
The damage caused by those cycles counted in Fig. 8(b) at each stress mean and range is calculated following the Model Code and listed in the matrix shown in Fig. 8(c), the total damage is the sum of those values shown in the damage matrix according to the Miner's rule [19].



(a)



(b)



(c)

Figure 8: (a) Stress history; (b) counted cycles for σ_c and (c) the corresponding damage caused (loaded with the train pulse ETR-Y, multiplied by 5).

Repeating this procedure for all the nodes in the central slab, a map for the fatigue damage is obtained and given in Fig. 9. We observe that the most unfavorable nodes are located around the middle of the slab track, under the central fastening cushions (below the third, fourth and fifth rail fastening devices).

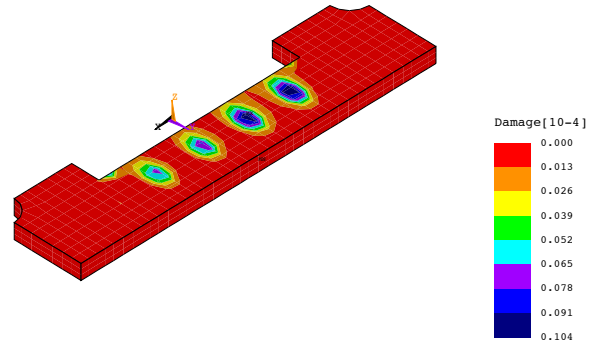


Figure 9: Fatigue damage map at the central slab (loaded with the train pulse ETR-Y, amplified by a factor of 5).

4 RESULTS FOR REAL HIGH-SPEED TRAIN PULSES

In this section, we show the results obtained for each kind of train that we have analyzed: AVE Class 103 and RENFE Class 120 -Alvia-. First the high-speed train load pulse is applied to the model in the transient analysis. Second, the corresponding stress and its time history are obtained for a node at the central slab and finally the fatigue damage map due to compression is plotted.

4.1 AVE Class 103 Train

The AVE Class 103 is a spanish high-speed train (trajectory Madrid-Barcelona), made and named as Velaro E by Siemens. It is of 200.84 m in total length and is composed of eight cars. Although the train could run with a speed of 350 km/h, the track is limited to 300 km/h. Figure 10 shows a typical load pulse of this high-speed train. Amplifying this pulse with a factor of 4, we obtain the results shown in Fig. 11. The most damaged region is located under the fourth fastening device. The stress history for this damaged node is represented in

Fig. 11(a). The damage map due to fatigue is shown in Fig. 11(b). A similar damage distribution to that of ETR-Y, see Fig. 9, is observed, though the maximum damage amounts to ten times more than that of ETR-Y.

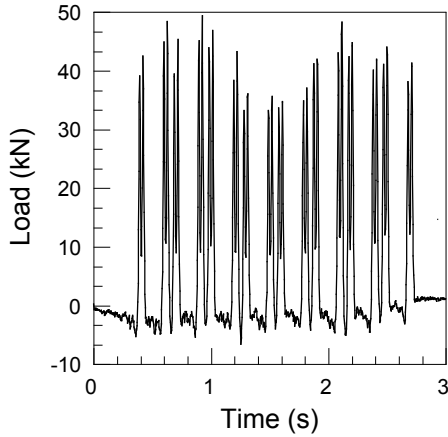


Figure 10: A typical load pulse for the train AVE S103.

4.2 Alvia Class 120 Train

The Alvia Class 120 is another type of train used for long distance service in Spain. It is composed of four coaches and has a total length of 106.23 m. It can run up to 250 km/h. A typical load pulse for this type of train is shown in Fig. 12.

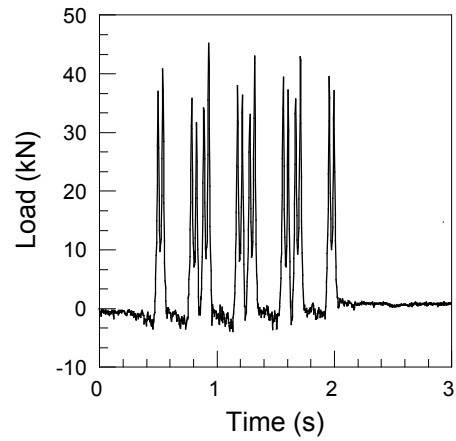
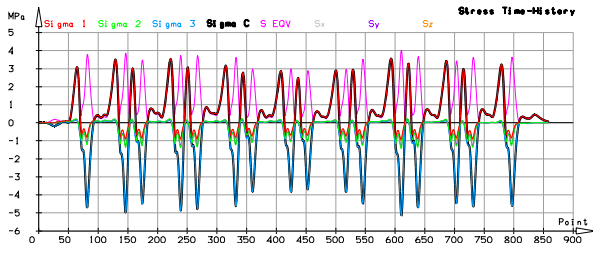
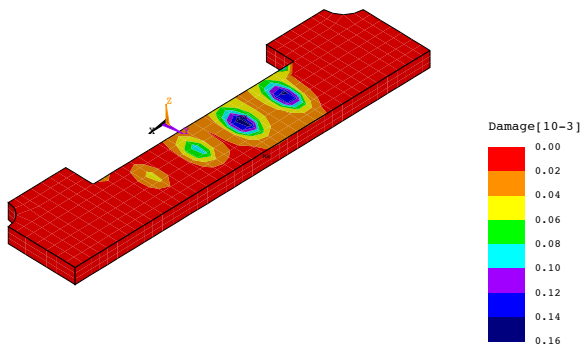


Figure 12: Alvia's train load pulse.

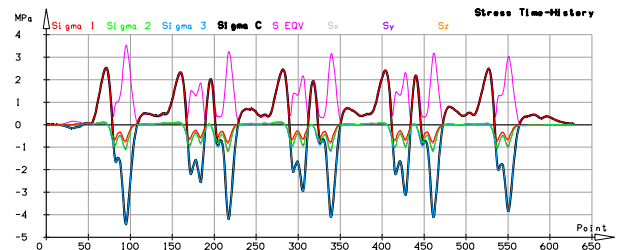


(a)

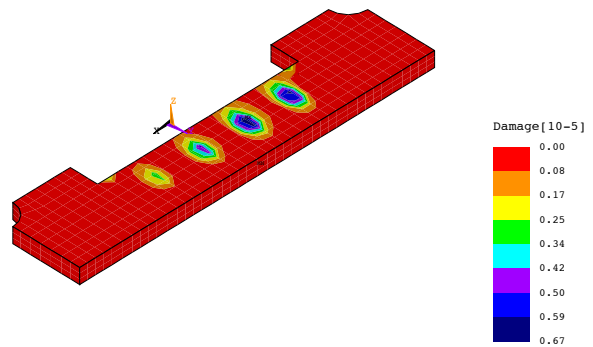


(b)

Figure 11: Results for AVE S103, load pulse amplified by a factor 4: (a) stress history for the most unfavorable node and (b) damage map.



(a)



(b)

Figure 13: Results for Alvia, load pulse amplified by a factor 4: (a) stress history for the most unfavorable node and (b) damage map.

After amplifying with a factor 4, the resulted stress history for the most unfavorable node and the fatigue map are respectively represented in Fig. 13(a) and Fig. 13(b). A similar damage distribution to that of ETR-Y and AVE S103, see Fig. 9 and Fig. 11(b), is observed, though the maximum damage is the smallest of the three.

5 PARAMETRIC ANALYSIS

In this section we analyze the influence of the concrete compressive strength, the fastening stiffness, the length of the fastening device, the elastic modulus of the cement-asphalt mortar and the slab thickness on the damage of the most unfavorable node.

First we look into the influence of the compressive strength of concrete by keeping constant the rest of the material parameters in Tab. 2. The load pulse is a more critical variant of the pulse shown in Fig. 10 multiplied by a factor 4 or 5. In Fig. 14 we show the result of this study by plotting the damage (solid lines) and fatigue life (dashed lines) of the most unfavorable node with respect to the compressive strength f_{ck} . The average traffic is assumed to be 60 trains per day. Notice that the damage decreases rapidly with the increase of f_{ck} . If a security coefficient of 4 is employed, f_{ck} should be no less than 50 MPa to guarantee a fatigue life of 100 years.

Next we study the sensitivity of the rest of the parameters on the damage of the most unfavorable node. In particular, the variation of the fastening stiffness is carried out by varying the elastic modulus of the fastening cushion

while keeping the rest unchanged. The influences of the fastening stiffness, the length of the fastening device, the modulus of the CA mortar and the slab thickness are respectively illustrated in the subfigures a, b, c and d of Fig. 15. It can be observed that, the damage value increases with the increase of the fastening stiffness, while decreases with the length of the fastening device. It needs to be remarked that, the damage value decreases to an asymptotic value with the increase of the modulus of the CA mortar layer; meanwhile, the damage does not vary much when the slab thickness increased from 0.17 m to 0.36 m. This implies that, if the rest were kept the same, the CA mortar layer can have a designed modulus as low as 60 to 80 MPa whereas the the slab track can be as thin as 0.17m.

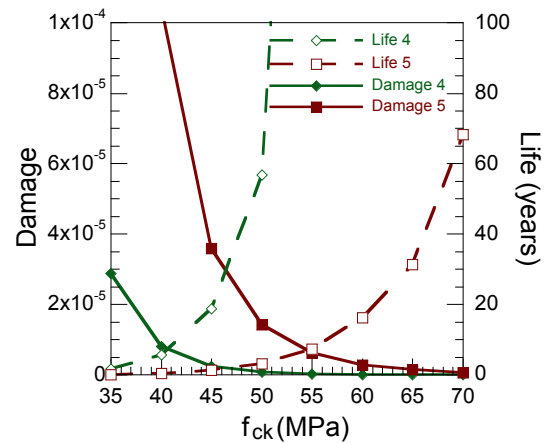


Figure 14: Damage and fatigue life of the most unfavorable node versus concrete compressive strength.

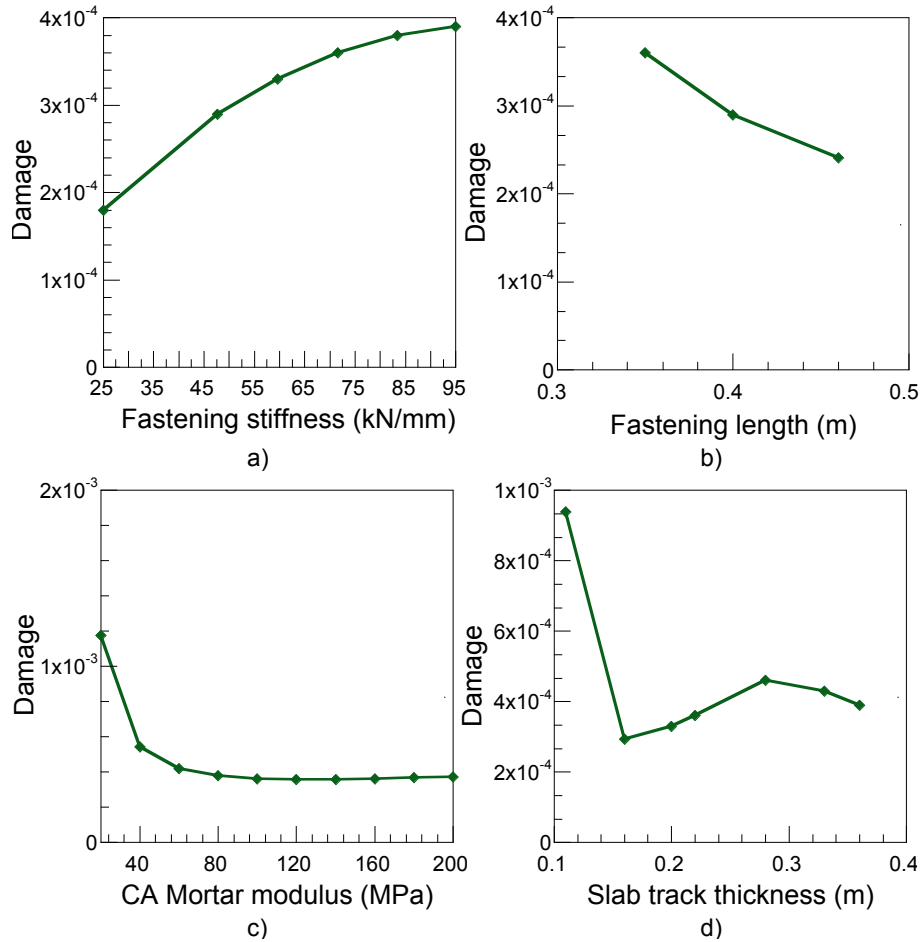


Figure 15: Damage of the most unfavorable node versus the fastening stiffness and the length of the fastening device, the elastic modulus of the cement asphalt mortar and the thickness of the slab.

6 CONCLUSION

We have modeled a three-slab track superstructure and the soil sub-grade in ANSYS to evaluate the fatigue behavior in the central slab. Numerical procedures are automated using the APDL script language. Modal analysis is performed to determine the fundamental modes and shapes. Transient analysis is carried out for a high-speed train load applied to the rail. Fatigue damage due to compression is evaluated following the Model Code. Since one train passage causes no damage, real train pulses from ETR-Y, AVE Class 103 and Alvia Class 120 multiplied by a factor 4 or 5 are applied to the rail for parametric studies. The damage map obtained shows that the unfavorable regions are located under the third to fifth fastening device.

The developed methodology is promising in

predicting the slab fatigue life and is particularly useful in optimizing the slab geometry and the superstructure. The current parametric study has suggested that

- for a security coefficient of four, the implied concrete should have a compressive strength no less than 50 MPa to give a 100-year fatigue life guarantee;
- the slab track thickness can be as thin as 0.17 m for a low level of fatigue damage;
- fatigue damage increases with the increase of the stiffness of the fastening device;
- for a low level of fatigue damage, the elastic modulus of the cement-asphalt-mortar layer can be as low as 60-80 MPa.

REFERENCES

- [1] S.D. Tayabji and D. Bilow. Concrete Slab Track State of the Practice. *Transportation Research Record: Journal of the Transportation Research Board*, 1742:87–96, 2001.
- [2] C. Esveld. *Modern Railway track, Second Edition*. Delft University of Technology, The Netherlands, 2001.
- [3] Esveld C. Recent developments in slab track. *European Railway Review*, 9:81–86, Jul 2003.
- [4] C. Jiang, J. Fan, and J.-J. Wang. Key techniques of ballastless track design on high-speed railway. *China Railway Science*, 25(2):42–47, April 2004.
- [5] S.A. Savidis and S. Bergmann. Slab track vibration and stress distribution induced by train passage. In C. Soize and G.I. Schüeler, editors, *EURODYN 2005*, volume 1-3, pages 651–656, 2005.
- [6] C. Cai and P. Xu. Dynamic analysis of key design parameters for ballastless track of high-speed railway. *Journal of Southwest Jiaotong University*, 45(4):493–497, Aug 2010.
- [7] X. Lei and B. Zhang. Analysis of Dynamic Behavior for Slab Track of High-Speed Railway Based on Vehicle and Track Elements. *Journal of Transportation Engineering, ASCE*, 137(4):227–240, April 2011.
- [8] M. Melis Maynar and F. J. González Fernández. *Ferrocarriles metropolitanos: tranvías, metros ligeros, y metros convencionales*. Colegio de Ingenieros de Caminos, Canales y Puertos, Madrid, 2004.
- [9] M. Melis Maynar. *Apuntes de introducción a la dinámica vertical de la vía y a las señales digitales en ferrocarriles*. Universidad Politécnica de Madrid, Madrid, 2008.
- [10] S.K. Kondapalli and D.N. Bilow. *Life cycle benefit of concrete slab track*. Portland Cement Association, 2008.
- [11] Railway Technical Research Institute. Outline of design standards for railway structures and commentary (earth structures). Technical report, Railway Bureau of the Ministry of Land Infrastructure and Transport Government of Japan, Aug. 2007.
- [12] M.J.M.M Steenbergen, A.V. Metrikine, and C. Esveld. Assessment of design parameters of a slab track railway system from a dynamic viewpoint. *Journal of Sound and Vibration*, 306:361–371, July 2007.
- [13] S. Zhu and C. Cai. Fatigue Life Prediction of CRTS I Ballastless Slab Track. *ICTE 2011-Proceedings of the Third International Conference on Transportation Engineering, ASCE*, pages 1714–1719, July 2011.
- [14] S.D. Downing and D.F. Socie. Simple rainflow counting algorithms. *International Journal of Fatigue*, 4(1):31–40, Jan 1982.
- [15] Inc. ANSYS. *Documentation for Release 12.1*. Swanson Analysis Systems IP, 2009.
- [16] W. Bösterling. Schienenbefestigungen für Feste Fahrbahnen ohne Betonschulter - das System 306 von Vossloh. *Boletín de Documentación Ferroviaria*, 4:37, 2009.
- [17] Ministerio de Fomento. Instrucción de acciones a considerar en el proyecto de puentes de ferrocarril (IAPF). Technical report, Dirección General de Ferrocarriles, Ministerio de Fomento, Gobierno de España, 2010.

- [18] FIB-Fédération Internationale du Béton. Model Code 2010 (first complete draft). *Materials*, 1(5):107–156, 2010.
- [19] M.A. Miner. Cumulative damage in fatigue. *Journal of Applied Mechanics*, 12:159–164, 1945.